Accepted by ApJL
Preprint typeset using LaTeX style emulateapj v. 5/2/11

arXiv:1601.03040v1 [astro-ph.SR] 12 Jan 2016

THE VLA NASCENT DISK AND MULTIPLICITY SURVEY: FIRST LOOK AT RESOLVED CANDIDATE DISKS AROUND CLASS 0 AND I PROTOSTARS IN THE PERSEUS MOLECULAR CLOUD

Dominique M. Segura-Cox[1], Robert J. Harris[1], John J. Tobin[2], Leslie W. Looney[1], Zhi-Yun Li[3], Claire Chandler[4], Kaitlin Kratter[5], Michael M. Dunham[6], Sarah Sadavoy[7], Laura Perez[4], Carl Melis[8]

Accepted by ApJL

ABSTRACT

We present the first dust emission results toward a sample of seven protostellar disk candidates around Class 0 and I sources in the Perseus molecular cloud from the VLA Nascent Disk and Multiplicity (VANDAM) survey with $\sim$0.05″ or 12 AU resolution. To examine the surface brightness profiles of these sources, we fit the Ka-band 8 mm dust-continuum data in the *u,v*-plane to a simple, parametrized model based on the Shakura-Sunyaev disk model. The candidate disks are well-fit by a model with a disk-shaped profile and have masses consistent with known Class 0 and I disks. The inner-disk surface densities of the VANDAM candidate disks have shallower density profiles compared to disks around more evolved Class II systems. The best-fit model radii of the seven early-result candidate disks are $R_c > 10$ AU; at 8 mm, the radii reflect lower limits on the disk size since dust continuum emission is tied to grain size and large grains radially drift inwards. These relatively large disks, if confirmed kinematically, are inconsistent with theoretical models where the disk size is limited by strong magnetic braking to < 10 AU at early times.

Subject headings: protoplanetary disks — stars: protostars

1. INTRODUCTION

Disks around young protostars are intrinsically linked to planet formation, binary formation, and protostellar mass accretion (Williams & Cieza 2011; Armitage 2011). In spite of their importance in star formation, when and how disks form–and their properties at early times–are poorly constrained. Hence, whether large and massive disks can form in young protostars (i.e. Class 0/I stages, André et al. 2000; Dunham et al. 2014) is subject to debate (e.g., Jørgensen et al. 2009; Chiang et al. 2008; Maury et al. 2010, respectively). Theoretical studies demonstrate magnetic fields can affect the formation timescales and properties of disks. In particular, strong magnetic fields can remove angular momentum from a collapsing envelope via magnetic braking, reducing forming disks to $R < 10$ AU (e.g., Mellon & Li 2008; Dapp & Basu 2010; Machida et al. 2011; Li et al. 2011; Dapp et al. 2012). Complicating the issue, several mechanisms can lessen the effects of magnetic braking, leading to larger disks: misalignment between the rotation axis and magnetic field of the system (e.g., Joos et al. 2012; Li et al. 2013), turbulence (e.g., Seifried et al. 2013; Joos et al. 2013), and initial conditions (e.g., Machida et al. 2014). The protostellar stage represents the stage with the largest mass reservoir available to form disks, therefore understanding the properties of disks at early epochs is crucial to determine the formation mechanism behind these structures.

Protostellar disks, however, are difficult to observe. Class 0 protostars and disks are so enshrouded that $\gtrsim$90% of their millimeter emission comes from the envelope (Looney et al. 2000). The three Class 0 protostars that have been observed with enough resolution and sensitivity to determine their disk properties and detect Keplerian rotation (L1527, VLA 1623, and HH212) have $R > 30$ AU disks, larger than expected from strong magnetic braking models (Ohashi et al. 2014; Tobin et al. 2012; Murillo et al. 2013; Codella et al. 2014). Observational limitations prevent smaller disks from being detected; these Class 0 disks may not represent typical disks at this stage of evolution. Class I protostars are less embedded and have cleared enough of their mass reservoir that more disks have been detected than in Class 0 systems (e.g., Harsono et al. 2014), though not as many disks have been revealed as in more-evolved Class II sources (e.g., Andrews et al. 2009, 2010). Without detection and study of more disks around the youngest protostellar systems, we cannot characterize early conditions of mass accretion onto the central protostar and planet formation because evolutionary mechanisms can change disk properties by the Class II phase (Williams & Cieza 2011).

To characterize the properties of the youngest disks and binaries, we are using the Karl G. Jansky Very Large Array (VLA) to conduct the VLA Nascent Disk and Multiplicity (VANDAM) continuum survey at $\lambda \sim 8, 10, 40, 64$ mm toward all identified protostars in the Perseus molecular cloud (Tobin et al. 2015a). The Perseus molecular cloud is relatively close (d $\sim$ 230 pc; Hirota et al. 2008, 2011) and has a significant number of Class 0 and I protostars (43 and 37 systems, respec-

[1] Department of Astronomy, University of Illinois, Urbana, IL 61801, USA; segurac2@illinois.edu
[2] Leiden Observatory, Leiden University, P.O. Box 9513, 2000-RA Leiden, The Netherlands
[3] Department of Astronomy, University of Virginia, Charlottesville, VA 22903, USA
[4] National Radio Astronomy Observatory, Socorro, NM 87801, USA
[5] Steward Observatory, University of Arizona, Tucson, AZ 85721, USA
[6] Harvard-Smithsonian Center for Astrophysics, Cambridge, MA 02138, USA
[7] Max-Planck-Institut für Astronomie, D-69117 Heidelberg, Germany
[8] Center for Astrophysics and Space Sciences, University of California, San Diego, CA 92093, USA

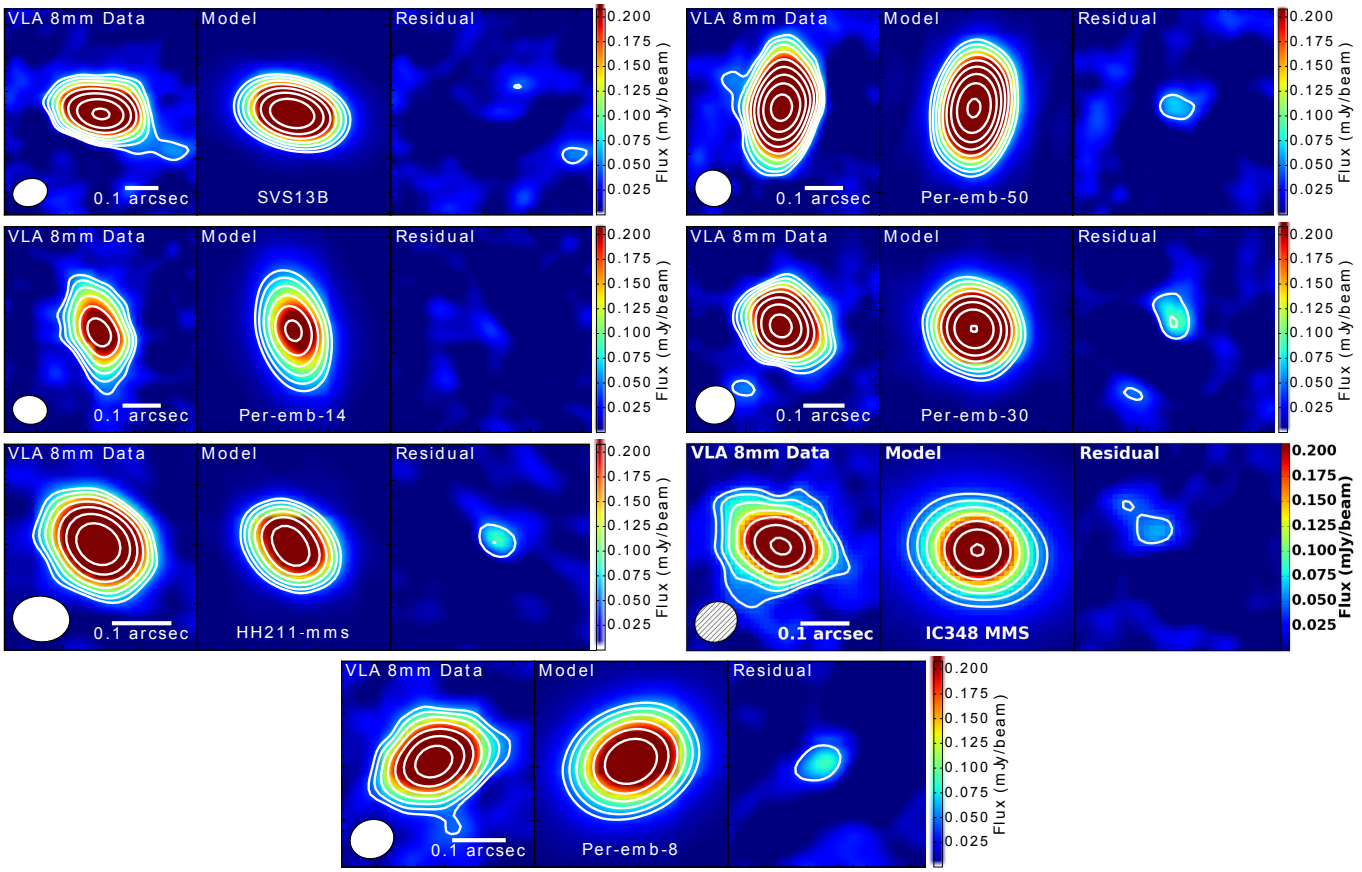

Figure 1. VLA A+B array data (left), $q = 0.25$ model from u,v-plane best-fit (center), and residual (right). Images were produced with robust = 0.25 weighting. Contours start at 3σ ($\sigma \sim 15\mu$Jy) with a factor of $\sqrt{2}$ spacing. The synthesized beam is in the lower left.

Table 1
Observations

Source	α (J2000)	δ (J2000)	A-array Obs. Date	B-array Obs. Date	Combined Beam (mas×mas)	Beam P.A. (°)
SVS13B	03:29:03.078	+31:15:51.740	03 May 2014	22 Oct 2013	105 × 83	-74.8
Per-emb-50	03:29:07.768	+31:21:57.125	01 Jun 2014	26 Oct 2013	97 × 94	54.0
Per-emb-14	03:29:13.548	+31:13:58.153	25 Feb 2014	22 Oct 2013	91 × 75	82.4
Per-emb-30	03:33:27.303	+31:07:10.161	16 May 2014	23 Oct 2013	99 × 92	-71.5
HH211-mms	03:43:56.805	+32:00:50.202	24 Feb 2014	21 Oct 2013	96 × 77	85.4
IC348 MMS	03:43:57.064	+32:03:04.789	23 Mar 2014	22 Oct 2013	89 × 80	-57.7
Per-emb-8	03:44:43.982	+32:01:35.209	22 Feb 2014	01 Oct 2013	82 × 72	-71.6

Note. — Observation dates mark the start of the observations. Combined beam sizes reflect robust = 0.25 weighting.

tively; Tobin et al. 2016, in press). The early results of the VANDAM survey have already revealed several candidate disk sources in both Class 0 and I sources at 10 AU scales. We consider these to be candidate disks because we lack kinematic data on small scales to determine whether these structures are rotationally supported. Nevertheless, so little is known about this early stage of disk evolution that even continuum-only imaging of young disks provides useful constraints on their properties.

In this Letter, we present the first results toward some of the protostellar disk candidates around Class 0 and Class I sources from the VANDAM survey. We show the observed structures are consistent with disks by fitting the 8 mm dust-continuum data in the u,v-plane to a simple, parameterized emission model based on the Shakura-Sunyaev disk model. VANDAM survey data provide an unparalleled opportunity to study the youngest disks: the unsurpassed resolution, sample size, and sensitivity for Class 0 and I protostars, permit a detailed examination of typical continuum properties of young disks.

2. OBSERVATIONS

The VANDAM survey includes Ka-band lower-resolution ($\sim$0.28″ or 65 AU) B-array data and high-resolution ($\sim$0.05″ or 12 AU) A-array data. We detected 16 protostellar candidate disk sources in the Perseus molecular cloud with the data collected in 2013, 2014, and 2015 (Segura-Cox et al. in prep). Here we focus on seven of the candidate disks (Table 1; Figure

Table 2
Source Data

Source	Class	Deconvolved Size (mas×mas)	Disk P.A. (°)	Disk Inclination (°)	F_{8mm} (μJy)	M_d ($M_\odot$)	$F_{>1700k\lambda}$ (μJy)
SVS13B	0	163×80	71.4±2.5	61	1352.7±11.6	0.14 - 0.29	82.0
Per-emb-50	I	137×53	170.0±0.3	67	1664.9±12.5	0.18 - 0.36	133.2
Per-emb-14	0	174×76	12.7±0.9	64	882.1±13.0	0.09 - 0.19	68.8
Per-emb-30	0	87×74	40.0±23.0	31	957.0±9.4	0.10 - 0.21	130.9
HH211-mms	0	93×59	34.8±9.6	51	867.5±8.1	0.09 - 0.19	42.9
IC348 MMS	0	145×105	70.8±2.2	44	1126.5±10.3	0.12 - 0.24	0.0
Per-emb-8	0	111×84	116.1±2.8	41	1120.7±10.3	0.12 - 0.24	126.5

Note. — Sizes and angles are measured from image-plane 2D Gaussian fits. Angles are measured counterclockwise from north. Uncertainties on the deconvolved sizes are ∼5.0 mas. Uncertainties on inclinations are ∼10°.

1, left) which were observed with A-array prior to 2015 and can be well modeled with the prescription described in Section 4. The observations were made in three-bit correlator mode, with a bandwidth of 8 GHz divided into 64 sub-bands. Each sub-band has 128 MHz bandwidth, 2 MHz channels, and full polarization products. The two 4 GHz basebands are centered at 36.9 GHz (∼8.1 mm) and 29.0 GHz (∼10.5 mm). Three sources were observed in each 3.5 hour block, and two sources were observed in each 2.75 hour block. Some observations were conducted as 1.5 hour blocks. 3C48 served as the flux calibrator, and 3C84 was the bandpass calibrator. The observations were taken in fast-switching mode to account for rapid atmospheric phase variations, with a 2.5 minute total cycle time to switch between the target source and the complex gain calibrator, J0336+3218. The total integration time on each source was ∼30 minutes for both A-array and B-array. We reduced the data with CASA 4.1.0 and the VLA pipeline (version 1.2.2). We executed additional flagging beyond pipeline flagging by inspecting the phase, gain and bandpass calibration solutions. VLA Ka-band data sets have an estimated amplitude calibration uncertainty of ∼10%, but only statistical uncertainties are considered in our analysis.

3. ESTIMATED MASSES

Two key quantities that describe disks are their masses and radii. While accurately determining disk radii requires modeling, masses are estimated from flux measurements (Table 2). By assuming optically thin emission, we estimate disk masses from the 8 mm dust continuum flux with the relation (Hildebrand 1983):

$$M = \frac{d^2 F_\nu}{B(T_d)\kappa_\nu}, \quad (1)$$

where F_ν, d, κ_ν, and $B_\nu(T_d)$, are respectively the total observed flux, distance, grain opacity, and blackbody intensity at dust temperature T_d. We estimate κ_ν at 8.1 mm by normalizing to Ossenkopf & Henning (1994) at 1.3 mm using a dust to gas ratio of 1/100: $\kappa_\nu = (1/100)(\nu/231\mathrm{GHz}))^\beta$ cm^2 g^{-1}. $\beta = 1$ is typically assumed for protostellar disks (Andrews et al. 2009), giving $\kappa_\nu = 0.00146$ cm^2 g^{-1}. Mass estimates are inherently ambiguous within an order of magnitude due to uncertainties in the dust-to-gas ratio, T_d, and β; rather than compute a single mass estimate, we calculate lower and upper mass estimates for each source by varying T_d. Lower masses were estimated by assuming $T_d = 40$ K, and we determined upper estimates using $T_d = 20$ K. These candidate disks range in flux from 867.5 μJy to 1664.9 μJy, providing estimated masses of 0.09–0.36 $M_\odot$ (Table 2).

4. MODELING

We modeled the 8 mm A+B array continuum data by fitting a symmetric disk intensity profile to the continuum emission of each source. In this modeling, we deprojected the 8 mm visibility data to a fixed position angle (P.A.) and fixed inclination as determined through image-plane 2D Gaussian fitting of the disk candidates and assumed the disks are circularly symmetric (Table 2). We azimuthally averaged the visibility data in the u,v-plane and binned the data in linearly spaced bins of width 50 kλ from 0 to 1500 kλ, switching to 30 log-spaced bins from 1500 to 4000 kλ where the data becomes noisier in order to boost the signal-to-noise level at large u,v-distances. We accounted for a lower-limit free-free point source component emanating from shocks in the protostellar jets (Anglada et al. 1998). Because point sources in the image domain have constant flux density at all u,v-distances, we account for the free-free component by calculating the average real component of the binned data with u,v-distance >1700 kλ and include the average as a flat, linear component of the model (Table 2); the profiles become flat at values >1700 kλ in all seven sources (e.g., Figure 2).

We fitted the real components of the deprojected, averaged, and binned profile to a simple disk model using a C-based implementation of `emcee`, an affine-invariant Markov chain Monte Carlo ensemble sampler (Goodman & Weare 2010; Foreman-Mackey et al. 2013). The imaginary components were assumed to be zero in the model since the disk is positioned at the phase center and assumed to be symmetric. The model mimics a Shakura-Sunyaev disk (Shakura & Sunyaev 1973) with a power law temperature profile; the resultant model disk surface brightness profile is

$$I(r) \propto \left(\frac{r}{R_c}\right)^{-(\gamma+q)} \exp\left\{-\left(\frac{r}{R_c}\right)^{(2-\gamma)}\right\}, \quad (2)$$

where $I(r)$ is the radial surface brightness distribution, q is the temperature exponent, γ is the power-law of the inner-disk surface density, and r is radius. R_c is a characteristic radius at which there is significant optical depth and disk material, making it a proxy for outer disk radius. This flux density profile is appropriate

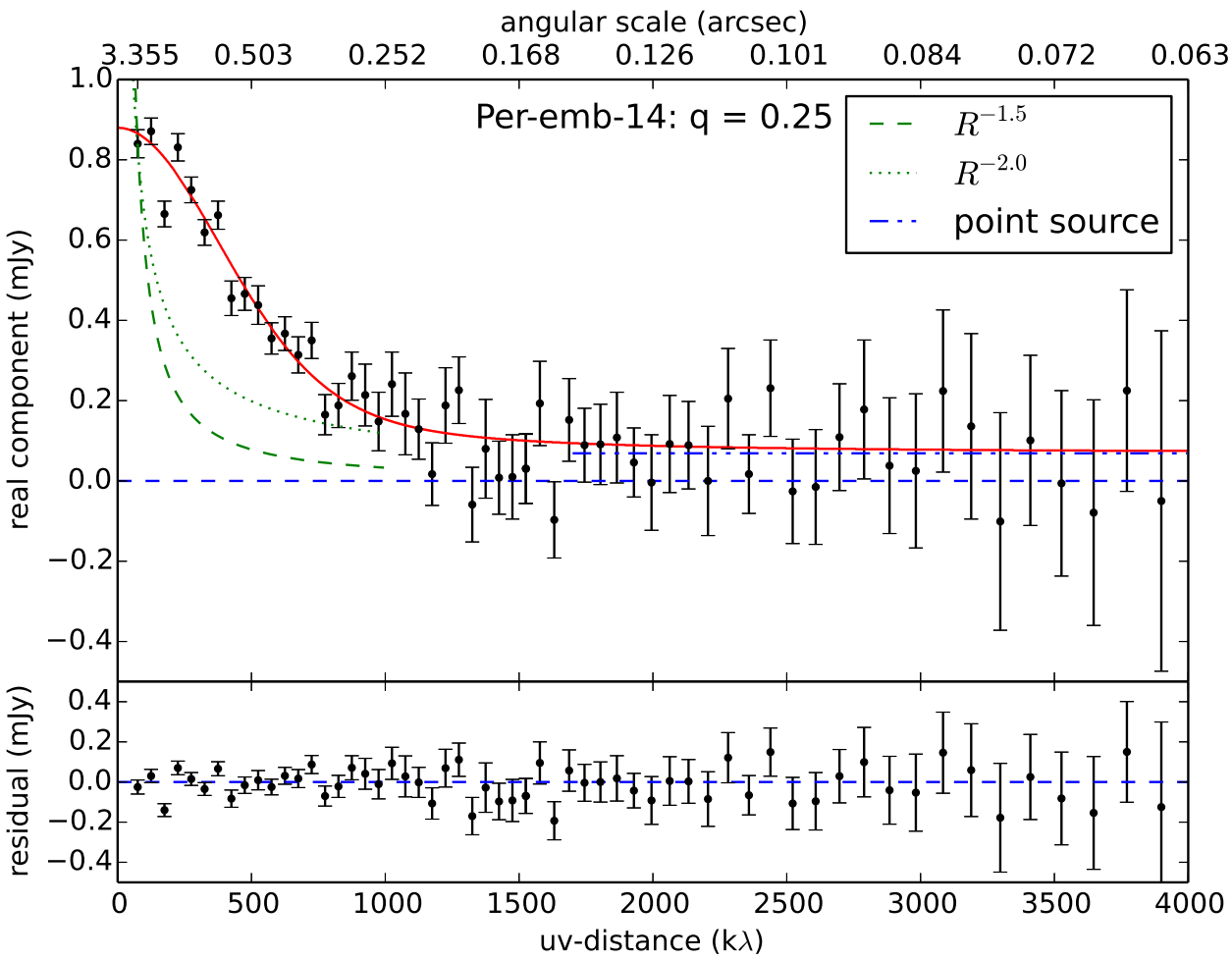

Figure 2. Sample real vs u,v-distance plot of 8 mm data. Top: real component of data. The blue dashed line indicates real component of zero. The red solid line is the best-fit model. Bottom: residual of real component minus model.

here because the 8 mm data is expected to be in the Rayleigh-Jeans tail of the dust emission. Flux is given by $F = \int_0^\infty I(r)\ 2\pi r\ dr$. Flux, disk radius, and gradient were free parameters in the fitting. We fitted a model disk for values of $q = [0.25, 0.50, 0.75, 1.00]$ to the observations in order to avoid over-fitting the data while exploring reasonable physical values of q.

5. RESULTS

Once model fitting was completed on the candidate disks, we generated disk model visibilities corresponding to the best-fit parameters. The best-fit model and residuals for each source were Fourier transformed, sampled at the same u,v-points as the data, and imaged using the same weighting as the data (Figure 1, center). We subtracted the model visibility from the data to produce a residual visibility set. Synthetic maps were created of the best-fit model disks. Residual maps were made by imaging the Fourier transformed visibilities after subtracting the model from the data in the u,v-plane (Figure 1, right). An example of the binned observational data, model fits, and residuals is also shown in Figure 2.

Fit results are shown in Table 3. The $\chi^2_{\rm reduced}$ values near one and the nearly empty residual maps indicate the seven candidate disk sources were well-modeled by our simple-shaped disk profile and are hence likely to be Class 0 and young Class I disks rather than inner envelope structure (Chiang et al. 2008). All candidate disks have modeled $R_c > 10$ AU, and except for HH211-mms the disks are large compared to the $R = 10$ AU upper limit predicted by magnetic braking models of Dapp & Basu (2010) at the Class 0 stage.

The model includes a disk and point-source component but does not take into account envelope emission. The observations filter out the majority of the contaminating envelope emission, demonstrated by the visibility profiles corresponding to $R^{-1.5}$ and $R^{-2.0}$ envelope surface density profiles plotted in Figure 2. These envelope density profiles represent, respectively, free-fall collapse and the singular isothermal sphere (Shu 1977). The best-fit models were determined from the maximum likelihood, i.e. the lowest χ^2 value, of all models fit to the data. Values of q near 0.5 are predicted by theory (e.g., Chiang & Goldreich 1997) for Class II protostars, which are more evolved than the protostars in our sample. Lower values of q result in lower values of $\chi^2_{\rm reduced}$ for six candidate disks. Values of $q < 0.5$ for

Table 3
8mm Best-fit Modeling Results

Source	q	γ	R_c (AU)	$\chi^2_{\rm reduced}$
SVS13B	0.25	$0.21^{+0.23}_{-0.20}$	$24.28^{+2.1}_{-1.7}$	2.194
	0.50	$0.42^{+0.25}_{-0.21}$	$25.50^{+1.9}_{-1.5}$	2.185
	0.75	$0.63^{+0.24}_{-0.22}$	$26.46^{+1.6}_{-1.4}$	2.175
	1.00	$0.85^{+0.26}_{-0.23}$	$27.28^{+1.4}_{-1.2}$	2.164
Per-emb-50	0.25	$0.08^{+0.02}_{-0.16}$	$21.9^{+0.8}_{-0.9}$	1.556
	0.50	$0.26^{+0.15}_{-0.17}$	$23.3^{+1.1}_{-1.0}$	1.558
	0.75	$0.44^{+0.16}_{-0.17}$	$24.6^{+1.4}_{-1.1}$	1.560
	1.00	$0.64^{+0.16}_{-0.18}$	$25.7^{+1.4}_{-1.3}$	1.563
Per-emb-14	0.25	$-0.11^{+0.16}_{-0.00}$	$28.5^{+2.3}_{-2.1}$	1.110
	0.50	$0.09^{+0.08}_{-0.21}$	$30.6^{+2.8}_{-2.3}$	1.114
	0.75	$0.27^{+0.17}_{-0.24}$	$32.5^{+2.2}_{-2.8}$	1.119
	1.00	$0.48^{+0.19}_{-0.23}$	$33.9^{+3.6}_{-3.1}$	1.123
Per-emb-30	0.25	$0.02^{+0.18}_{-0.31}$	$14.0^{+1.0}_{-0.9}$	1.100
	0.50	$0.20^{+0.04}_{-0.32}$	$14.9^{+1.9}_{-1.1}$	1.102
	0.75	$0.39^{+0.30}_{-0.34}$	$15.8^{+1.9}_{-1.3}$	1.104
	1.00	$0.59^{+0.14}_{-0.33}$	$16.5^{+31.3}_{-1.6}$	1.107
HH211-mms	0.25	$0.48^{+0.40}_{-0.78}$	$10.5^{+0.8}_{-0.8}$	1.009
	0.50	$0.65^{+0.43}_{-0.82}$	$11.0^{+1.0}_{-0.9}$	1.009
	0.75	$0.81^{+0.42}_{-0.79}$	$11.5^{+1.2}_{-1.2}$	1.009
	1.00	$1.01^{+0.44}_{-0.81}$	$11.9^{+1.4}_{-1.3}$	1.009
IC348 MMS	0.25	$-0.58^{+0.11}_{-0.11}$	$25.7^{+2.8}_{-2.2}$	1.085
	0.50	$-0.39^{+0.19}_{-0.11}$	$29.0^{+3.2}_{-2.6}$	1.096
	0.75	$-0.19^{+0.11}_{-0.27}$	$31.6^{+4.1}_{-2.9}$	1.107
	1.00	$0.02^{+0.07}_{-0.11}$	$33.7^{+4.3}_{-3.1}$	1.118
Per-emb-8	0.25	$0.01^{+0.16}_{-0.19}$	$19.0^{+1.2}_{-1.1}$	1.099
	0.50	$0.20^{+0.17}_{-0.20}$	$20.2^{+1.4}_{-1.3}$	1.107
	0.75	$0.40^{+0.17}_{-0.21}$	$21.2^{+1.6}_{-1.4}$	1.114
	1.00	$0.61^{+0.17}_{-0.20}$	$22.1^{+1.8}_{-1.6}$	1.122

Note. — Values of q are fixed. Values of γ and R_c are determined from best-fit models. Uncertainties reflect 90% confidence intervals.

Class 0 and younger Class I sources are favored since the envelope mass reservoir is still large, and radiation is reprocessed from the protostar and directed back onto the disk, increasing the brightness of the outer disk relative to the inner regions of the disk and flattening the brightness distribution (D'Alessio 1996). Compared to the other modeled protostars, $\chi^2_{\rm reduced}$ is notably higher for SVS13B which may be a more complicated source and not well described by the model.

6. DISCUSSION

The estimated masses of the candidate disks are consistent with known disks around Class 0 and I protostars. The seven VANDAM candidate Class 0 and I disks range in estimated masses of 0.09–0.36 $M_\odot$. Scaling to our value of κ_ν, Class 0 protostar L1527's disk is 0.013 $M_\odot$ (Tobin et al. 2013) with $T_d = 30$ K. A recent interferometric study of Class I disks in Taurus (Harsono et al. 2014) revealed the disks around TMC1A, TMC1, TMR1 and L1536 to have masses of 0.4–3.3$\times10^{-2}$ $M_\odot$ with T_d = 30 K and Ossenkopf & Henning (1994) opacities. All mass estimates have uncertainties of a factor of ∼10 due to the unknown gas-to-dust ratio, T_d, β, and varying choices of κ_ν.

Values of γ, the power-law of the inner-disk surface density, for the VANDAM sources can be compared to values found for older Class II sources. The best-fit models for our seven sources yield $-0.58 < \gamma < 0.45$. Negative values of γ indicate increasing surface density with radius, inconsistent with disks, yet for all sources at least one value of q exists which produces a positive best-fit γ (Table 3). Andrews et al. (2010) determined γ at 880 μm for disks around Class II objects using a two-dimensional parametric model with a prescription of the surface density profile similar to the radial surface brightness distribution applied in this Letter. The Class II sources have values of $0.4 < \gamma < 1.1$, larger than VANDAM results. The modeled, surface density profiles of the Class 0 and I systems taper off less quickly with radius compared to the Class II systems inside the characteristic radius R_c.

The best-fit model radii of the candidate Class 0 disks are between ∼15-30 AU, except HH211-mms with R_c ∼ 10 AU. These are smaller than the Keplerian disks found in L1527 and VLA 1623 at 1.3 mm (Ohashi et al. 2014; Murillo et al. 2013, $R \sim 54$ AU and $R \sim 189$ AU respectively) but consistent with the size of HH212 (Codella et al. 2014, R > 30 AU). The modeled radii (Table 3) are a factor of 1 to 1.5 times larger than the deconvolved sizes (Table 2). The radii of the new candidate disks may represent lower limits on disk sizes because continuum emission from dust is biased by dust grain size. Radial drift (Birnstiel et al. 2010; Weidenschilling 1977) sends large grains inward in the disk, and so the long wavelength observations preferentially trace inner disk emission (Pérez et al. 2012). We expect the 8 mm dust-modeled radii to be less than the gas disk radius, and so the 8 mm radii are lower-limits on disk size; multi-wavelength observations that include gas tracers are required to further constrain disk radii. Per-emb-14 was resolved at 1.3 mm by Tobin et al. (2015b) with $R \sim 100$ AU; thus the disk is indeed likely larger than the 8 mm radius quoted here. In all cases, the previously known disks and new candidate Class 0 disks are larger than the expected upper limit of 10 AU from strong magnetic braking models (e.g., Dapp & Basu 2010).

The seven VANDAM candidate disks are well-fit by a disk-shaped model and have disk masses, values of γ, and radii consistent with known disks. These candidate disks can be compared to the well-studied Class 0 systems with disks: L1527 (Tobin et al. 2012) and VLA 1623 (Murillo & Lai 2013). L1527 and VLA 1623 have large Keplerian disks ($R \sim 50$ AU, Ohashi et al. 2014; Murillo et al. 2013) as well as misaligned magnetic fields and rotation axes (Hull et al. 2014), suggesting that misaligned fields and large disks may be linked (Segura-Cox et al. 2015). The discrepancy between theoretical and observed disk sizes could be due to misalignment between the magnetic field and rotation axis, which changes the strength of magnetic braking, allowing disks to grow at early times (Hennebelle & Ciardi 2009; Joos et al. 2012; Li et al. 2013; Krumholz et al. 2013). Similarly, aligned orientations would strengthen magnetic braking and limit disk size, as seen in Class 0 source B335 with a disk of $R < 5$ AU (Yen et al. 2015; Hull et al. 2014). The large Keplerian Class 0 disks and new candidate disks indicate significant magnetic braking either has already occurred, has not happened, or the magnetic field is weak enough for disks with $R > 10$ AU around these Class 0 protostars to form, though other configurations are possible.

It is illustrative to compare the presence of VANDAM candidate disks to the magnetic field morphology of the systems. The TADPOL survey examines protostellar dust polarization and hence plane-of-sky magnetic field orientation. (Hull et al. 2014). For sources with detected magnetic fields, we are able to determine which systems have misaligned orientations between the outflow (a proxy for rotation axis) and the average magnetic field orientation. The magnetic field morphologies of two of the seven VANDAM sources in this Letter (HH211-mms and SVS13B) were also examined as a part of the TADPOL survey. A qualitative comparison between the VANDAM data and the TADPOL magnetic field orientation reveals that HH211-mms and SVS13B morphologies agree with the tentative link between $R > 10$ AU disks and misaligned orientations (Segura-Cox et al. 2015). HH211-mms has a clearly misaligned orientation (Hull et al. 2014), agreeing with theoretical predictions that disks with $R > 10$ AU disks form at early times in systems with non-parallel orientations. SVS13B has a more complicated magnetic field morphology with an average aligned orientation (Hull et al. 2014) with the outflow (Bachiller et al. 1998), however the TADPOL data has lower resolution than our data ($\sim 3''$, or 700 AU), and the innermost regions of the magnetic field has misaligned orientation near the candidate disk. The small-scale, misaligned orientation in SVS13B could be caused by magnetic fields being wrapped up with the rotating disk, and the aligned magnetic field lines further from the disk are less influenced by the disk wrapping.

7. CONCLUSIONS

The first results of the VANDAM survey revealed new candidate Class 0 and I disks in continuum emission in the Perseus molecular cloud and is the most sensitive, most complete, and highest resolution survey of young protostellar disks to-date. For seven of the VANDAM systems, we fit the deprojected, averaged, and binned data in the u,v-plane to a disk-shaped profile, accounting for a free-free point source potentially contaminating the dust emission, to affirm the disk candidacy of the sources and to begin to model disk properties. To confirm that these disks are true, rotationally-supported disks, kinematic follow-up observations are required. The seven VANDAM candidate disks are well-fit by a model with a disk-shaped profile and have masses comparable to known disks. The inner-disk surface densities of the Class 0 and I candidate disks taper off less quickly with radius than their Class II counterparts.

The best-fit model radii of the new candidate disks are $R_c > 15$ AU, except HH211-mms with $R_c \sim 10$ AU. Since magnetic braking is expected to suppress Class 0 disks to $R < 10$ AU, this suggests that magnetic braking has already ended or is inconsequential in some Class 0 sources. At 8 mm, the modeled radii are lower limits on the disk size since dust continuum emission is tied to grain size and large grains radially drift inwards in the disk; the actual sizes of the disks may be larger. Multi-wavelength observations are needed to put added constraints on disk radii. Furthermore, theory predicts larger disk growth in systems with misaligned outflow axes and magnetic field orientations, and the early VANDAM candidate disk results combined with polarization data for two of the sources indicate that indeed $R > 10$ AU disks have formed in systems with misaligned orientations.

This research made use of APLpy, an open-source plotting package for Python hosted at http://aplpy.github.com.

DMSC is currently supported by NRAO Student Observing Support grant SBC NRAO 2015-06997. JJT is currently supported by grant 639.041.439 from the Netherlands Organisation for Scientific Research (NWO). ZYL is supported by NASA NNX14AB38G and NSF AST-1313083.

The National Radio Astronomy Observatory is a facility of the National Science Foundation operated under cooperative agreement by Associated Universities, Inc.

REFERENCES

André, P., Ward-Thompson, D., & Barsony, M. 2000, in Protostars and Planets IV, 59
Andrews, S. M., Wilner, D. J., Hughes, A. M., et al. 2009, ApJ, 700, 1502
Andrews, S. M., Wilner, D. J., Hughes, A. M., et al. 2010, ApJ, 723, 1241
Anglada, G., Villuendas, E., Estalella, R., et al. 1998, AJ, 116, 2953
Armitage, P. J., 2011, ARA&A, 49, 195
Bachiller, R., Guilloteau, S., Gueth, F., et al. 1998, A&A, 339, 49
Birnstiel, T., Ricci, L., Trotta, F., et al. 2010, A&A, 516, 14
Chiang, E. I. & Goldreich, P. 1997, ApJ, 490, 368
Chiang, H.-F., Looney, L. W., Tassis, K., et al. 2008, ApJ, 680, 474
Codella, C., Cabrit, S., Gueth, F., et al. 2014, A&A, 568, 5
D'Alessio, P. 1996, PhD thesis, Univ. Nacional Astónoma de México
Dapp, W. B., & Basu, S. 2010, A&A, 521, L56
Dapp, W. B., Basu, S., & Kunz, M. W., 2012, A&A, 541, A35
Dunham, M. M., Stutz, A. M., Allen, L. E., et al. 2014, Protostars and Planets VI, 195
Foreman-Mackey, D., Hogg, D. W., Lang, D., Goodman, J. 2013 PASP, 125, 306
Goodman, J. & Weare, J., 2010, Comm. App. Math. Comp. Sci., 5, 65
Harsono, D., Jørgensen, J. K., van Dishoeck, E. F., et al. 2014, A&A, 562, 77
Hennebelle, P., & Ciardi, A. 2009, A&A, 506, 29
Hildebrand, R. H. 1983, QJRAS, 24, 267
Hirota, T., Bushimata, T., Choi, Y. K., et al. 2008, PASJ, 60, 37
Hirota, T., Honma, M., Imai, H., et al. 2011, PASJ, 63, 1
Hull, C. L. H., Plambeck, R. L., Kwon, W., et al. 2014, ApJS, 213, 13
Joos, M., Hennebelle, P., & Ciardi, A. 2012, A&A, 543, A128
Joos, M., Hennebelle, P., Ciardi, A. & Fromang, S. 2013, A&A, 554, A17
Jørgensen, J. K., van Dishoeck, E. F., Visser, R., et al. 2009, A&A, 507, 861
Krumholz, M. R., Crutcher, R. M., & Hull, C. L. H. 2013, ApJ, 767, L11
Li, Z.-Y., Krasnopolsky, R., & Shang, H. 2011, ApJ, 738, 180
Li, Z.-Y., Krasnopolsky, R., & Shang, H. 2013, ApJ, 774, 82
Looney, L. W., Mundy, L. G., & Welch, W. J. 2000, ApJ, 529, 477
Machida, M. N., Inutsuka, S.-I., & Matsumoto, T. 2011, PASJ, 63, 555
Machida, M. N., Inutsuka, S.-I., & Matsumoto, T. 2014, MNRAS, 438, 2278
Maury, A. J., André, P., Hennebelle, P., et al. 2010, A&A, 512, 40

Mellon, R. R., & Li, Z.-Y. 2008, ApJ, 681, 1356
Murillo, N. M., & Lai, S.-P. 2013, ApJL, 764, L15
Murillo, N. M., Lai, S.-P., Bruderer, S., et al. 2013, A&A, 560, 103
Ohashi, N., Saigo, K., Aso, Y., et al. 2014, ApJ, 796, 131
Ossenkopf, V., & Henning, T. 1994, A&A, 291, 943
Pérez, L. M., Carpenter, J. M., Chandler, C. J., et a., 2012, ApJL, 760, L17
Segura-Cox, D. M., Looney, L. W., Stephens, I. W., et al. 2015, ApJ, 798, L2
Seifried, D., Banerjee, R., Pudritz, R. E., & Klessen, R. S. 2013, MNRAS, 432, 3320
Shakura, N. I., Sunyaev, R. A. 1973, A&A, 24, 337
Shu, F. H.1977, ApJ, 214, 488
Tobin, J. J., Bergin, E. A., Hartmann, L., et al. 2013, ApJ, 765, 18
Tobin, J. J., Hartmann, L., Chiang, H.-F., et al. 2012, Nature, 492, 83
Tobin, J. J., Looney, L. W., Li, Z.-Y., et al. 2016, ApJ, in press
Tobin, J. J., Dunham, M. M., Looney, L. W, et al. 2015a, ApJ, 798, 61
Tobin, J. J., Looney, L. W., Wilner, D. J., et al. 2015b, ApJ, 805, 125
Weidenschilling, S. J. 1977, MNRAS, 180, 57
Williams, J. P. & Cieza L. A., 2011, ARA&A, 49, 67
Yen, H.-W., Koch, P. M., Takakuwa, S., et al. 2015, ApJ, 799, 193